Exploring Multiscale Causal Interventions for Burned Area Estimation

Amir Mustofa Irawan[1,4], Mercè Vall-llossera[1,3], Carlos López-Martínez[1,3], Adriano Camps[1,2,3], Gerard Portal[3], Miriam Pablos[1], Alberto Alonso-González[1]

[1]CommSensLab – UPC, Department of Signal Theory and Communications, Universitat Politècnica de Catalunya (UPC), 08034 Barcelona, Spain – amir.mustofa.irawan@upc.edu, miriam.pablos@upc.edu, alberto.alonso-gonzalez@upc.edu

[2]ASPIRE Visiting International Professor, UAE University CoE, 15551 Al Ain, UAE – Adriano.jose.camps@upc.edu

[3]Institut d'Estudis Espacials de Catalunya IEEC, 08034 Barcelona, Spain - merce.vall-llosera@upc.edu, carlos.lopezmartinez@upc.edu, gerard.portal@upc.edu

[4]Department of Climatology, Indonesia State College of Meteorology, Climatology, and Geophysics (STMKG), Tangerang Selatan, Indonesia

Keywords: Burned area, causal graph, PCMCI, do-calculus.

Abstract

Understanding complex causal interactions between local, continental, and global drivers remains a significant challenge in wildfire prediction systems. This study implements a causal inference framework combining the Peter-Clark momentary conditional independence (PCMCI) algorithm with do-calculus interventions to analyse land-atmosphere feedback mechanisms influencing wildfire dynamics across South Asia (India, Pakistan, Myanmar, and adjacent regions). Time-series causal graphs derived from satellite and reanalysis data identified 500-hPa geopotential height anomalies (ΔZ_{500}) as the primary driver of surface aridity and wildfire incidence. Extreme scenario simulations via do-operator perturbations revealed that artificially enhancing ΔZ_{500} to the 100th percentile, representing intensified upper-tropospheric ridging, produced the most severe mean burned area outcomes. Under these conditions, mean extreme burned area reached ~4.2 log ha (~15,000 ha), exceeding impacts from other perturbed variables. The integration of PCMCI-derived causal networks with counterfactual analysis provides a novel methodology for disentangling multiscale wildfire drivers, offering critical insights into future climate-driven fire risks through explicit representation of teleconnection mechanisms.

1. Introduction

Wildfires pose serious risks to human safety, economic stability, and ecosystems, with climate change intensifying their impact. Building on prior research, this study investigates the causal structure between Earth systems and wildfires using data-driven modeling. It applies the Peter–Clark algorithm with momentary conditional independence (PCMCI) to uncover causal links in time series. Unlike previous studies focused on fire presence (Prapas et al., 2023), this work simulates how changes in input variables affect burned area size, providing valuable insights into the magnitude of direct and indirect interactions.

Recent developments in causal discovery methods, such as the PCMCI, have made it possible to detect lagged causal links within multivariate time series, thereby improving the interpretability of wildfire forecasting models (Runge et al., 2019). Incorporating causal reasoning into wildfire modelling has proven valuable, not only for enhancing predictive accuracy but also for shedding light on the mechanisms driving fire regimes amid evolving climate conditions. Utilizing causal inference techniques allows researchers to explore hypothetical scenarios and evaluate the effects of interventions like vegetation management or fire suppression, supporting the creation of data-informed strategies for wildfire risk reduction (Carriger et al., 2021).

The rationale for employing PCMCI and do-calculus in this wildfire modelling study stems from their capacity to reveal true causal connections, moving beyond simple statistical associations. PCMCI is particularly adept at reconstructing causal networks in complex time series datasets, as it reduces the risk of false positives caused by autocorrelation and confounding factors (Runge et al., 2019). In parallel, do-calculus, based on Pearl's framework for causal inference, facilitates the estimation of causal effects and supports counterfactual analysis under various interventions (Pearl, 2009a), which is essential for understanding how environmental drivers shape wildfire activity. Unlike traditional deep learning (DL) models, which often act as opaque "black boxes" with limited transparency (Reichstein et al., 2019), these causal techniques generate interpretable causal graphs and offer deeper insights into the processes influencing wildfire behaviour. This interpretability enhances their robustness and adaptability, especially in the context of non-stationary climate patterns where DL models may falter due to their dependence on historical correlations rather than underlying causal dynamics (Rudin, 2019). Furthermore, instead of merely predicting fire occurrence as in previous work by (Zhao et al., 2024), this study investigates how modifications to input variables impact the overall extent of burned areas.

2. Study Area

This research utilizes a comprehensive collection of global datasets on wildfire drivers and burned area, integrating information from three sources covering the period from 2011 to 2020. All data are harmonized onto a uniform spatial and temporal grid (0.25° × 0.25°, with eight-day intervals). The focus area for this investigation is South Asia, specifically within the coordinates 5°–38°N and 59°–99°E. The choice of this region is driven by its recent history of intense wildfire activity. Notably, the occurrence of extreme wildfire events increased by a factor of 2.2 between 2003 and 2023, with six of the most significant episodes in India taking place over the last seven years (Cunningham et al., 2024). In addition, Nepal faced an extraordinary wildfire season in spring 2021, experiencing active fires at a frequency ten times above the long-term average observed from 2002 to 2020. This surge in fire activity followed

an extended period of rainfall shortage and severe drought that began after the monsoon season in October 2020 (Pokharel et al., 2023).

The study region is characterized by pronounced climatic and ecological diversity, featuring complex topography and a rich assortment of vegetation types. Climate zones range from the humid tropics of southern India and Myanmar, to the arid and semi-arid landscapes of Pakistan and western India, and the cooler, temperate areas of northern India (Verma, 2021). The broad spectrum of vegetation, spanning tropical rainforests, deciduous forests, grasslands, and desert ecosystems, reflects the region's varied environmental conditions, with each vegetation type distributed according to local climate and terrain (Champion and Seth, 1968).

3. Dataset

This study uses a compilation of global data on fire drivers and burned areas from three separate datasets spanning the years 2011 to 2020, all aligned on a consistent spatio-temporal grid (0.25° × 0.25° with eight-day intervals). Anomaly values, denoted with Δ in this study, are calculated to remove the seasonality (Irawan et al., 2024). Local scale (X_l) inputs are obtained from SeasFire Cube (Karasante et al., 2023), including total precipitation anomalies (ΔTP), vapor pressure deficit anomalies (ΔVPD), and normalized difference vegetation index anomalies (ΔNDVI). Soil moisture anomalies (ΔSM), are taken from the Soil Moisture and Ocean Salinity Level 3 (SMOS L3) products. At the continental scale (X_c), this study selects two tropospheric variables from ERA5 climate reanalysis (Hersbach et al., 2020): 500-hPa geopotential height anomalies (ΔZ_{500}), and the 300-hPa meridional wind component (v_{300}). Additionally, North Atlantic Oscillation (NAO) and El Niño-Southern Oscillation (ENSO) data from SeasFire Cube are used to explain global climate indices (X_g). The target variable is a value of global burned area (BA) from SeasFire Cube.

4. Methodology

The Peter–Clark (PC) algorithm (Spirtes and Glymour, 1991), a widely used constraint-based method, is applied to construct directed acyclic graphs (DAGs) by identifying causal relationships through conditional independence tests. The process follows these steps:

1) *Initialize:* Begin with a fully connected undirected graph representing potential causal relationships.

2) *Conditional Independence Testing*: Test each variable pair X_t^i, X_t^j given a conditioning set Z. If they are conditionally independent, remove the edge.

3) *Iterate:* Increase the size of Z and repeat until all variable pairs have been tested.

4) *Edge Orientation:* Identify v-structures (colliders) and apply rules to direct edges while preventing cycles.

The PCMCI framework relies on conditional independence tests of the form $\mathrm{CI}(X_{t-\tau}^i, X_t^j, S)$ to determine whether $(X_{t-\tau}^i \perp\!\!\!\perp X_t^j \mid S)$, given a specified conditioning set S. The TIGRAMITE software package (Runge, 2017) provides multiple options for conducting these independence tests. To improve recall, the PCMCI method (Runge et al., 2019) integrates momentary conditional independence (MCI) tests, capturing time-delayed causal effects where a cause at $t-\tau$ influence effects at t. MCI systematically evaluates all variable pairs X_t^i and X_t^j, and computes the conditional independence $\mathrm{CI}(X_{t-\tau}^i, X_t^j \mid S)$, where the conditioning set S is composed of the union of the parent sets $P(X_t^j)$ and $P(X_{t-\tau}^i)$, as estimated during the PC phase. The set $P(X_{t-\tau}^i)$ s constructed by shifting the parent variables of X^i backward by τ timestep. In cases where $X_{t-\tau}^i \epsilon P(X_t^j)$, it is excluded from the conditioning set to avoid conditioning on the variable under test. Link assumptions are used to determine the orientation of certain edges, with the ordering based on the climate scale, progressing from the global to the local scale. Based on the spatial scale of climate change and its impacts (Wilbanks and Kates, 1999), the influence of global emissions and atmospheric driving forces cascades downward to affect local-scale ecosystems. Therefore, in cases of conflicting orientations, this study reverses the direction to ensure the correct orientation. The conditional independence test applied in this study uses partial correlations (ParCorr). A maximum time delay ($\tau_{\max}$ = 10, ~3 months) is considered as proposed in the previous result (Goswami et al., 2022), and a significance level $\alpha = 0.05$ is used to threshold the estimated matrix of p-values and construct the causal graph.

In the context of time series analysis, this study assume that variables follow a temporal order and satisfy the assumptions of

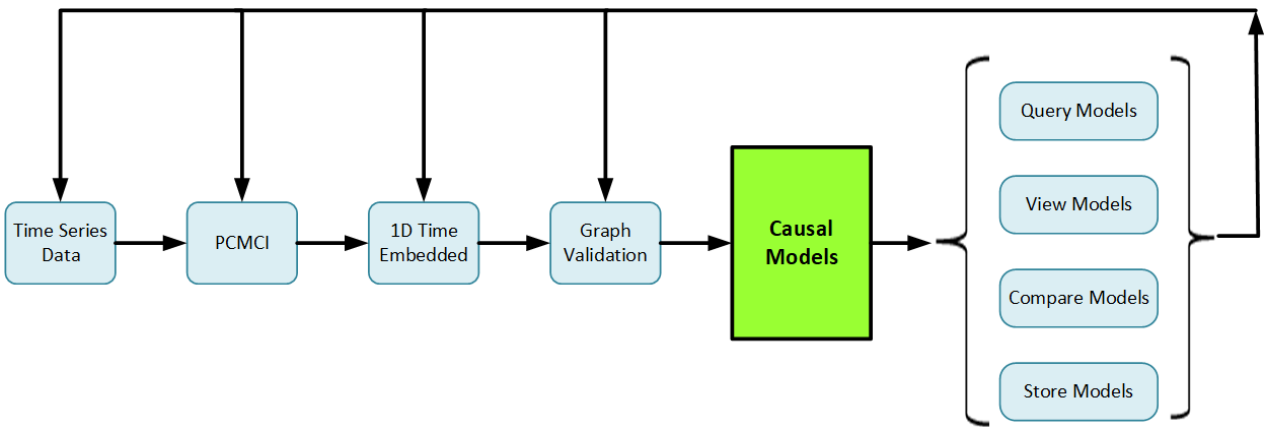

Fig. 1. Workflow of the proposed causal model. The input time series data include local, continental, oceanic, and climatic index variables, each characterized by different temporal and spatial scales. Interventions can be performed through the "Query Models" on the causal model. Adapted from Cooper et al., (2015).

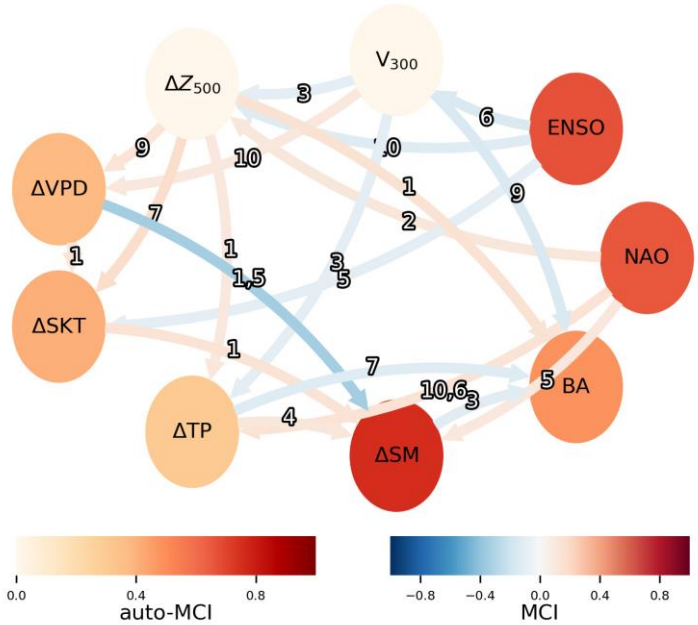

Fig. 2. Causal network visualization for South Asia. The color of each connecting line (MCI) represents the strength and type of causal link: red lines indicate positive relationships, while blue lines signify negative ones. Numbers on the arrows specify the time lag between variables, given in eight-day increments, and the arrowheads show the direction of causality. Node colors (auto-MCI) illustrate the degree of autocorrelation present in each variable’s time series.

the causal Markov condition (LMC), faithfulness assumption (TPa), causal sufficiency, and causal stationarity, while also excluding any contemporaneous causal relationships (Runge, 2018). The validation of directed acyclic graphs (DAGs) in causal inference fundamentally depends on two key assumptions: the LMC and the TPa. The LMC ensures that a node is conditionally independent of its non-descendants given its parents, while the TPa states that d-separated variables in the graph should be conditionally independent in the data. Violations of these assumptions indicate potential errors in the DAG. A permutation-based framework is used to test these assumptions by comparing the given DAG against randomly permuted ones, establishing a statistical baseline (Pearl, 2009b). Additionally, the random common cause approach introduces covariates to assess the DAG's stability, ensuring that causal estimates remain robust.

Given an outcome y, its value depends on one or more specific features. The $do(\cdot)$ operator calculates the probability that $Y = y$ conditioned to the input variable X_t being held constant at $X_t = x_t$ (Pearl, 1994). This do-calculus allows for the intentional manipulation of the selected variable by fixing it at a specific state or value, thereby excluding all other possible states and their associated data. This is typically expressed as $P\left(y \middle| do(X_t = x_t)\right)$. Since PCMCI is designed to uncover causal relationships across different time lags, an autoencoder approach was used to perform temporal embedding, compressing information from various time lags into a one-dimensional space. The encoder layer reduces the multi-time-lagged input of each variable into a compact latent representation. The decoder subsequently restores the input by transforming this latent space back into the original feature dimensions. The data was then mapped back onto the original latitude and longitude grid to calculate the intervention. The intervention scenario is implemented with the input variable bootstrapped and set to the 25th, 50th, 75th, and 100th percentiles to simulate the impact of the input variables, ranging from minimum to worst-case conditions (represented by the 100th percentile), on the size of the burned area. The method proposed in this study is summarized in Figure 1.

5. Result

Causal networks were generated using the PCMCI algorithm applied to 2011–2020 datasets to establish directional links between input and output variables, integrating both spatial and temporal dimensions. As demonstrated in Fig. 2, PCMCI effectively identifies delayed teleconnections between the El Niño–Southern Oscillation (ENSO, quantified via SOI indices) and upper-atmospheric circulation anomalies (ΔZ_{500} and v_{300}) over South Asia, with response lags of 6 and 10 months, respectively. These relationships align with previously validated atmospheric dynamics (An and Goswami, 2022). The analysis reveals a robust inverse relationship between SOI values and aridity indicators (ΔVPD and ΔSKT), where negative SOI phases (El Niño conditions) correlate with heightened surface dryness.

The PCMCI analysis further reveals that the North Atlantic Oscillation (NAO) exerts a positive causal influence on precipitation patterns within the study region. This aligns with prior findings demonstrating NAO’s correlation with enhanced winter rainfall in northwestern India (Hunt and Zaz, 2023). The results also indicate that positive NAO phases amplify the upper-level pressure gradient (ΔZ_{500}) over South Asia, strengthening the subtropical jet stream’s intensity. Additionally, PCMCI identifies a marked increase in vapor pressure deficit (ΔVPD), driven by warming-induced atmospheric desiccation linked to soil moisture deficits, as a key factor strongly associated with expanded burned

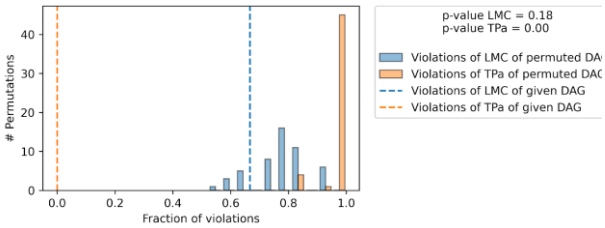

Fig. 3. Evaluation of directed acyclic graph (DAG).

areas, corroborating earlier mechanistic analyses (Williams et al., 2019).

The methodology was implemented within the Structural Causal Model (SCM) framework, leveraging causal networks identified through the PCMCI algorithm. SCM formalizes causal relationships by structuring variables as nodes in a directed acyclic graph (DAG), with edges representing direct causal dependencies. Each variable is expressed through structural equations that incorporate only its direct causal antecedents (parent nodes), ensuring alignment with the underlying data-generating mechanisms. By iteratively estimating variables through these equations, the framework propagates causal effects across the system, disentangling direct, indirect, and confounded influences on burned area dynamics. Interventional calculus techniques were then applied to quantify variable-specific causal impacts, enabling predictive counterfactual analysis of wildfire behavior under hypothetical conditions.

To optimize causal representation, three regression approaches were tested: gradient-boosted decision trees, polynomial regression with feature transformation, and standard linear regression. Gradient-boosted trees achieved the lowest mean squared error (MSE = 0.14 log hectares), outperforming polynomial regression (MSE = 0.24) and linear regression (MSE = 0.29). The strong performance of the gradient-boosted approach highlights its capacity to model complex nonlinear causal interactions in wildfire spread. A coefficient of determination ($R^2 = 0.54$) indicates the model explains moderate variance in burned area, suggesting additional refinements could improve explanatory power.

To assess the robustness of causal assumptions, the original causal network underwent 50 permutations to produce randomized directed acyclic graphs (DAGs). For each randomized version, violation rates for the Local Markov Condition (LMC) and Time-series Parental (TPa) assumptions were quantified. Fig. 3 illustrates the resulting violation distributions across permutations, with LMC deviations shown in blue and TPa deviations in orange. Vertical dashed lines depict the baseline violation rates observed in the non-permuted DAG, providing a reference for evaluating statistical significance.

As illustrated in Fig. 3, a p-value of 0.18 for the LMC indicates that the observed fraction of violations of this condition in the given DAG is 82% lower than the lowest value observed in any of the 50 randomly permuted DAGs. This suggests that the structure of the original DAG is highly consistent with the LMC, and that the dependencies modelled by the graph align closely with the true conditional independence relations in the data. Similarly, the TPa, which posits that all conditional independencies present in the data should also be reflected in the structure of the DAG, yields a p-value ≤ 0.0001. This means that the given DAG also has significantly fewer violations of the faithfulness assumption than the randomly permuted DAGs, further supporting the idea that the original DAG is a valid representation of the causal relationships in the data (Bozcuk and Alemdar, 2024).

The causal model integrates probabilistic and interventional interpretations, employing Pearl’s do-operator to simulate interventions by conditioning on parent variables within the causal network. For example, interventions were applied to continental-scale drivers (ΔZ_{500}, v_{300}) and local factors (ΔVPD, ΔSM) to quantify their relative impacts on burned area extremes. Input variables were systematically adjusted to percentile thresholds (25th, 50th, 75th, 100th) to model the effects of conditions ranging from baseline to worst-case scenarios.

As shown in the heatmap in Fig. 4, the intervention analysis reveals distinct causal pathways:

- Soil moisture (ΔSM): At the 100th percentile (extremely wet conditions), burned area decreases markedly due to suppressed flammability.
- Geopotential height anomalies (ΔZ_{500}): Maximum values (intense upper-level ridges) drive the most pronounced surge in extreme mean burned area magnitude, around log 5 ha (~15,000 ha).
- Vapor pressure deficit (ΔVPD): Elevated ΔVPD increases fire activity at the 100th percentile, though less dramatically than ΔZ_{500}.
- Meridional wind (v_{300}): High v_{300} values correlate with northward airflow from the Indian Ocean, enhancing moisture transport and rainfall, thereby reducing fire risk across the study region.

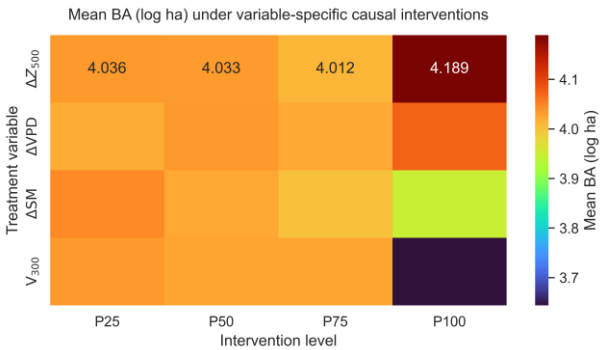

Fig. 4. Heatmap analysis of the logarithmic values of the potential extreme mean burned area after applying bootstrapping and intervening on the input variables set at the 25th, 50th, 75th, and 100th percentiles, simulating the influence of these variables across a range from minimal to worst-case scenarios (with the latter represented by the 100th percentile).

The causal network (Fig. 2) and intervention results collectively identify ΔZ_{500} as the dominant driver of surface desiccation and extreme fire spread. Mechanistically, heightened ΔZ_{500} fosters persistent high-pressure systems that trap heat, amplifying heatwave intensity and fuel aridity (Irawan et al., 2024). These findings emphasize the need for wildfire prediction systems that holistically account for multiscale interactions between global teleconnections, regional atmospheric dynamics, and local environmental conditions.

6. Conclusion

This study presents a causal discovery framework combining PCMCI with structural causal modelling to analyse wildfire

drivers using Earth observation data. The approach generates hierarchical causal networks that separate direct and indirect fire influences, improving transparency and reliability compared to purely statistical models. By embedding physical mechanisms into the causal graph, the methodology captures how upper-tropospheric variables, particularly 500-hPa geopotential height anomalies (ΔZ_{500}) and 300-hPa meridional wind (v_{300}), directly and indirectly modulate burned area across South Asia. Indirect effects propagate through intermediate surface variables, including skin temperature, vapor pressure deficit, precipitation, and soil moisture. Critically, results emphasize the multifactorial nature of wildfire causation, rejecting single-driver explanations.

Validation metrics (LMC/TPa p-values) confirm the causal network’s statistical robustness against randomized permutations, demonstrating its capacity to resolve conditional dependencies. The framework advances process-based wildfire modeling by linking macroscale atmospheric dynamics to local fire behaviour through explicit causal pathways. Future work will focus on merging adaptive causal discovery with deep learning architectures to develop predictive models that maintain physical consistency while leveraging data-driven pattern recognition.

Acknowledgements

The project that gave rise to these results received the support of a fellowship from the ”la Caixa” Foundation (ID 100010434), with fellowship code LCF/BQ/DI21/11860028. This work was also supported by Project PID2020-114623RB-C32 funded by MCIN/ AEI /10.13039/501100011033 and Project PID2023-149659OB-C22 funded by MCIU /AEI /10.13039/501100011033 / FEDER, UE.

References

An, S.-I., Goswami, B., 2022. An assessment of the ENSO-monsoon teleconnection in a warming climate. https://doi.org/10.21203/rs.3.rs-2101241/v1

Bozcuk, H.Ş., Alemdar, M.S., 2024. Solving the puzzle of quality of life in cancer: integrating causal inference and machine learning for data-driven insights. Health Qual. Life Outcomes 22, 60. https://doi.org/10.1186/s12955-024-02274-7

Carriger, J.F., Thompson, M., Barron, M.G., 2021. Causal Bayesian networks in assessments of wildfire risks: Opportunities for ecological risk assessment and management. Integr. Environ. Assess. Manag. 17, 1168–1178. https://doi.org/10.1002/ieam.4443

Champion, S.H.G., Seth, S.K., 1968. A Revised Survey of the Forest Types of India. Manager of Publications.

Cunningham, C.X., Williamson, G.J., Bowman, D.M.J.S., 2024. Increasing frequency and intensity of the most extreme wildfires on Earth. Nat. Ecol. Evol. 8, 1420–1425. https://doi.org/10.1038/s41559-024-02452-2

Goswami, B.N., Chakraborty, D., Rajesh, P.V., Mitra, A., 2022. Predictability of South-Asian monsoon rainfall beyond the legacy of Tropical Ocean Global Atmosphere program (TOGA). Npj Clim. Atmospheric Sci. 5, 58. https://doi.org/10.1038/s41612-022-00281-3

Hersbach, H., Bell, B., Berrisford, P., Hirahara, S., Horányi, A., Muñoz-Sabater, J., Nicolas, J., Peubey, C., Radu, R., Schepers, D., Simmons, A., Soci, C., Abdalla, S., Abellan, X., Balsamo, G., Bechtold, P., Biavati, G., Bidlot, J., Bonavita, M., De Chiara, G., Dahlgren, P., Dee, D., Diamantakis, M., Dragani, R., Flemming, J., Forbes, R., Fuentes, M., Geer, A., Haimberger, L., Healy, S., Hogan, R.J., Hólm, E., Janisková, M., Keeley, S., Laloyaux, P., Lopez, P., Lupu, C., Radnoti, G., De Rosnay, P., Rozum, I., Vamborg, F., Villaume, S., Thépaut, J., 2020. The ERA5 global reanalysis. Q. J. R. Meteorol. Soc. 146, 1999–2049. https://doi.org/10.1002/qj.3803

Hunt, K.M.R., Zaz, S.N., 2023. Linking the North Atlantic Oscillation to winter precipitation over the Western Himalaya through disturbances of the subtropical jet. Clim. Dyn. 60, 2389–2403. https://doi.org/10.1007/s00382-022-06450-7

Irawan, A.M., Vall-llossera, M., López-Martínez, C., Camps, A., Chaparro, D., Portal, G., Pablos, M., Alonso-González, A., 2024. Land, jet stream, and other atmospheric effects on burned area estimation during the South Asian heatwave of 2022. Int. J. Appl. Earth Obs. Geoinformation 128, 103720. https://doi.org/10.1016/j.jag.2024.103720

Karasante, I., Alonso, L., Prapas, I., Ahuja, A., Carvalhais, N., Papoutsis, I., 2023. SeasFire as a Multivariate Earth System Datacube for Wildfire Dynamics. https://doi.org/10.48550/ARXIV.2312.07199

Pearl, J., 2009a. Causality, 2nd ed. Cambridge University Press, Cambridge. https://doi.org/10.1017/CBO9780511803161

Pearl, J., 2009b. Causality: Models, Reasoning, and Inference, 2nd ed. Cambridge University Press. https://doi.org/10.1017/CBO9780511803161

Pearl, J., 1994. A Probabilistic Calculus of Actions, in: de Mantaras, R.L., Poole, D. (Eds.), Uncertainty in Artificial Intelligence. Morgan Kaufmann, San Francisco (CA), pp. 454–462. https://doi.org/10.1016/B978-1-55860-332-5.50062-6

Pokharel, B., Sharma, S., Stuivenvolt-Allen, J., Wang, S.-Y.S., LaPlante, M., Gillies, R.R., Khanal, S., Wehner, M., Rhoades, A., Hamal, K., Hatchett, B., Liu, W.-Y., Mukherjee, S., Aryal, D., 2023. Amplified drought trends in Nepal increase the potential for Himalayan wildfires. Clim. Change 176, 17. https://doi.org/10.1007/s10584-023-03495-3

Prapas, I., Bountos, N.I., Kondylatos, S., Michail, D., Camps-Valls, G., Papoutsis, I., 2023. TeleViT: Teleconnection-driven Transformers Improve Subseasonal to Seasonal Wildfire Forecasting. https://doi.org/10.48550/ARXIV.2306.10940

Reichstein, M., Camps-Valls, G., Stevens, B., Jung, M., Denzler, J., Carvalhais, N., Prabhat, 2019. Deep learning and process understanding for data-driven Earth system science. Nature 566, 195–204. https://doi.org/10.1038/s41586-019-0912-1

Rudin, C., 2019. Stop explaining black box machine learning models for high stakes decisions and use interpretable models instead. Nat. Mach. Intell. 1, 206–215. https://doi.org/10.1038/s42256-019-0048-x

Runge, J., 2018. Causal network reconstruction from time series: From theoretical assumptions to practical estimation. Chaos Interdiscip. J. Nonlinear Sci. 28, 075310. https://doi.org/10.1063/1.5025050

Runge, J., 2017. TIGRAMITE-Causal discovery for time series datasets.

Runge, J., Nowack, P., Kretschmer, M., Flaxman, S., Sejdinovic, D., 2019. Detecting and quantifying causal associations in large nonlinear time series datasets. Sci. Adv. 5, eaau4996. https://doi.org/10.1126/sciadv.aau4996

Spirtes, P., Glymour, C., 1991. An Algorithm for Fast Recovery of Sparse Causal Graphs. Soc. Sci. Comput. Rev. 9, 62–72. https://doi.org/10.1177/089443939100900106

Verma, O., 2021. Climate Change and Its Impacts with Special Reference to India, in: Taloor, A.K., Kotlia, B.S., Kumar, K. (Eds.), Water, Cryosphere, and Climate Change in the Himalayas, Geography of the Physical Environment. Springer International Publishing, Cham, pp. 39–55. https://doi.org/10.1007/978-3-030-67932-3_3

Wilbanks, T.J., Kates, R.W., 1999. Global Change in Local Places: How Scale Matters. Clim. Change 43, 601–628. https://doi.org/10.1023/A:1005418924748

Williams, A.P., Abatzoglou, J.T., Gershunov, A., Guzman-Morales, J., Bishop, D.A., Balch, J.K., Lettenmaier, D.P., 2019. Observed Impacts of Anthropogenic Climate Change on Wildfire in California. Earths Future 7, 892–910. https://doi.org/10.1029/2019EF001210

Zhao, S., Prapas, I., Karasante, I., Xiong, Z., Papoutsis, I., Camps-Valls, G., Zhu, X.X., 2024. Causal Graph Neural Networks for Wildfire Danger Prediction. https://doi.org/10.48550/ARXIV.2403.08414